

PASSIVE AEROGRAVITY ASSISTED TRAJECTORIES FOR A MARS ATMOSPHERIC SAMPLE RETURN MISSION

Evgeniy Sklyanskiy*, Tung-Han You[†],
Neil Cheatwood[‡], Alicia Dwyer Cianciolo[§] and Angela Bowes^{**}

A number of studies have demonstrated that aerodynamic lift during a planetary low-altitude atmospheric flyby can increase the V_{∞} bending angle and the total ΔV achievable from gravity assist. Aero-Gravity Assist (AGA) trajectories of this type require a significantly high spacecraft L/D (lift-to-drag) ratio and a fairly robust closed-loop guidance algorithm capable of providing a desired control authority for level, nearly constant-altitude atmospheric flight. The AGA concept has been described in some previous publications as one of the techniques for Mars and Venus atmospheric sample return mission design strategies¹⁻⁴. Recent analysis has demonstrated that passive, ballistic (zero-lift) aeropass trajectories could equally satisfy potential future sample return mission objectives and provide quite robust and simple alternatives to a complex guided AGA lifting trajectory design.

INTRODUCTION

A sample returned from Mars is one NASA's highest priorities. This paper focuses on a subclass of Mars Sample Return (MSR) conceptual missions whose primary objective would be to collect an atmospheric sample and return it safely to Earth. Based on the previous studies, this mission class would rely on the performance of Waverider vehicles which must perform an AGA maneuver in the lower altitude bend of planetary atmosphere⁵⁻⁸. The AGA technique is very similar to the Gravity Assist (GA) method of reducing the propellant requirements for planetary transfer, where the gravitational attraction of a planet helps to bend the trajectory of a spacecraft and therefore change the heliocentric velocity with no propulsive ΔV . The AGA maneuver has the same objective, but in addition to gravitational force it uses aerodynamic lift to produce additional trajectory bending which makes the interplanetary trajectory design more flexible. Earlier papers provide the reference Earth-Mars-Venus-Earth AGA trajectories and discuss a potential application of a Waverider vehicle for atmospheric sample return missions⁹⁻¹². The mechanical design of the Waverider spacecraft assumes a hypersonic slender body vehicle

*Engineer, Entry, Descent, and Landing / Guidance and Control Systems Group, Jet Propulsion Laboratory, California Institute of Technology, Pasadena, California 91109

[†]Group Supervisor, Inner Planet Navigation – Mission Design and Navigation Section, Jet Propulsion Laboratory, California Institute of Technology, Pasadena, California 91109

[‡]Senior Engineer, Atmospheric Flight & Entry Systems Branch, NASA Langley Research Center, Hampton, Virginia 23681

[§]Engineer, Atmospheric Flight & Entry Systems Branch, NASA Langley Research Center, Hampton, Virginia 23681

^{**}Engineer, Atmospheric Flight & Entry Systems Branch, NASA Langley Research Center, Hampton, Virginia 23681

© Copyright 2011 California Institute of Technology. Government sponsorship acknowledged.

capable of mitigating high heat rates and achieving a high Lift-to-Drag ratio (L/D), which is essential for a prolonged atmospheric flight and effective trajectory bending maneuver. Unfortunately, the Technology Readiness Level (TRL) of hypersonic vehicles that can effectively perform an AGA maneuver at $L/D > 3$ is low. Hence, the mission implementation of the Waverider concept in the near future is somewhat unrealistic.

An excellent alternative to the AGA mission scenario is a passive ballistic (zero-lift) aeropass trajectory which could satisfy future sample return mission objectives and which is simpler and more robust than a guided AGA lifting trajectory design. Unlike AGA, the passive aeropass scenario could be accomplished with a conventional spacecraft design protected by a heatshield, while the mission architecture would not require an extensive development and could be configured for 2016-2018 Earth-Mars launch opportunities. With minimum technology development, atmospheric sample return missions using a passive aeropass concept could be extremely cost-effective. This paper provides a detailed study of various Earth-Mars-Earth mission trajectory designs primarily focused on 2016-2020 Mars aeropass opportunities. A detailed Monte Carlo analysis of the aeropass maneuver addresses the ΔV uncertainties associated with the propulsive burn necessary for the Earth return portion of the trajectory.

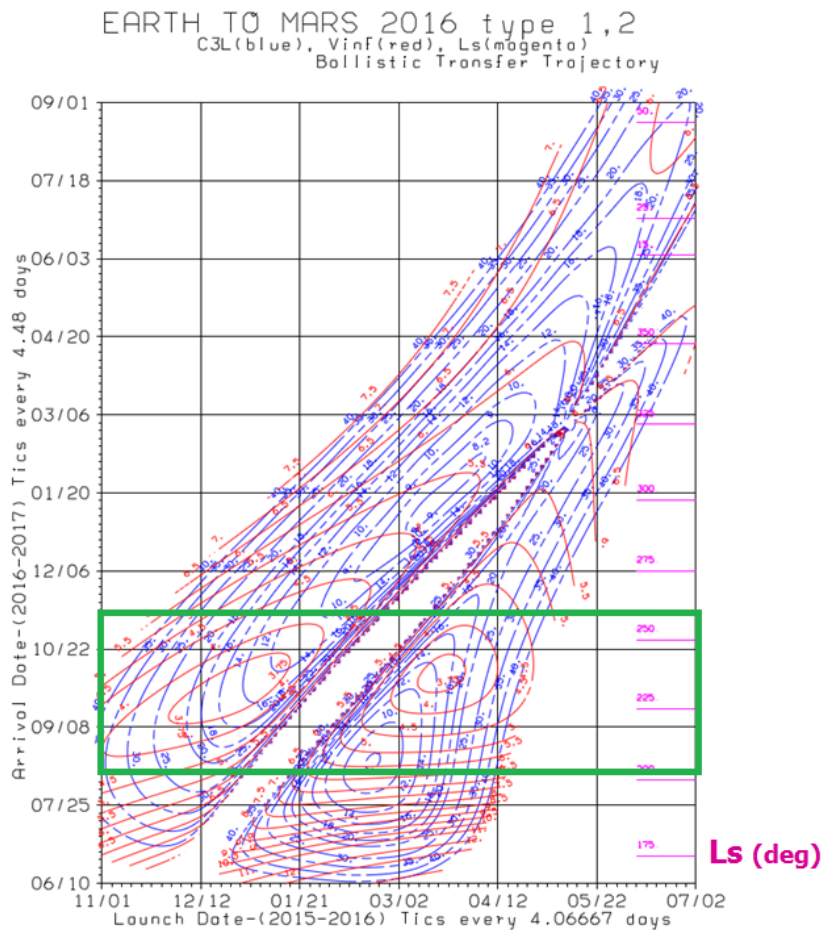


Figure 1. 2016 Earth-Mars Type I/II ballistic trajectories with V_∞ constraint

DESIGN STRATEGY

The 2016-2018 Mars arrival opportunities were selected for developing a set of Earth-Mars-Earth reference trajectories used in this conceptual study. The first objective was to methodically analyze the entire design space for Earth-Mars 2016 and 2018 launch/arrival pairs. Based on the family of ballistic trajectories the orbital transfer energy plots (also known as “pork-chop” plots) suggest that both *Type I/II* and *Type III-IV*- Earth-Mars trajectories could potentially work for the outbound portion of an EME trajectory design (See Figures 1-2)¹³. The search space was limited further by setting the Mars arrival V_∞ constraint to be less than 5 km/s. Although the study is purely conceptual, based on the Pathfinder¹⁴ EDL experience (i.e. the highest entry speed recorded during the atmospheric entry at Mars, $V_{rel}=7.48$ km/s) the feasibility of the atmospheric flyby in low Martian atmosphere suggests that the inertial entry velocity should be constrained to 7.0 km/s ($V_\infty < 5$ km/s) to keep the maximum heat rate/loads of the heatshield protecting the spacecraft within design limits. A more detailed discussion about a vehicle dynamics during the atmospheric flyby will be given in the subsequent section *Mars Aeropass Trajectory Analysis*.

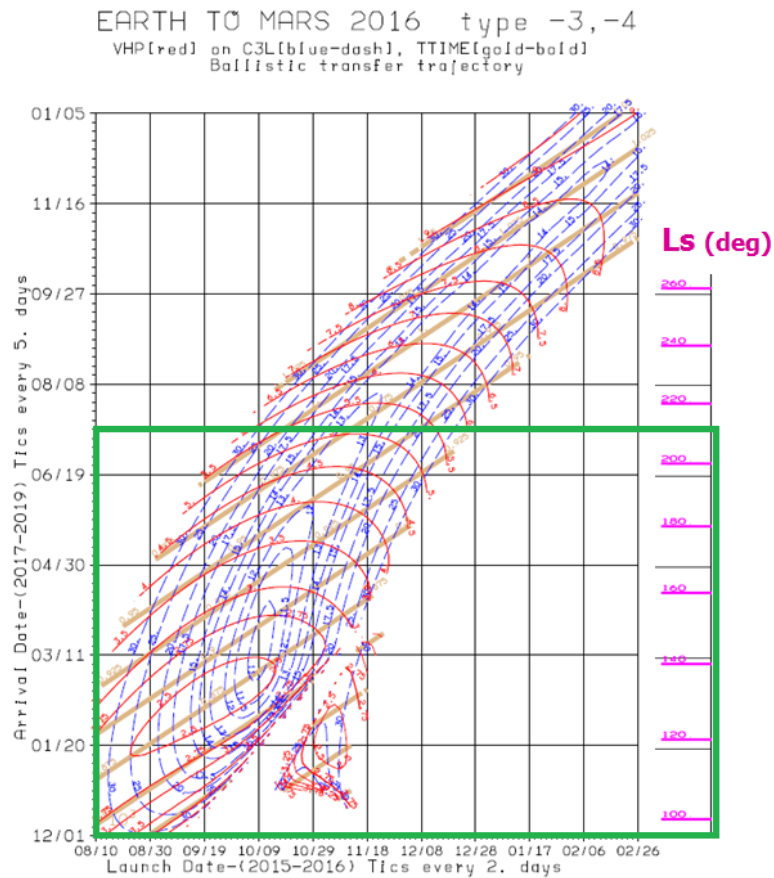


Figure 2. 2016 Earth-Mars Type III-IV- ballistic trajectories with V_∞ constraint

The energy plots provided reliable starting guesses and, while referring to the illustrated set of Earth launch/Mars arrival pairs, the next step in the design process was to connect the Earth-Mars

ballistic trajectory segments with the Earth return portion of a trajectory. Based on the heliocentric two-body nature of the problem it was decided to use MIDAS¹⁵, a patched conic, impulsive interplanetary optimization program. This software was written in FORTRAN and was originally developed to investigate a variety of complex ballistic heliocentric transfer trajectories. MIDAS is intended to be used for preliminary mission feasibility studies where a relatively accurate estimate of mission performance is more important than high model accuracy. The optimization algorithm of this program is configured by default to minimize the total weighted mission ΔV . MIDAS has the capability of adding or deleting deep space maneuvers and powered planetary swing-by maneuvers as dictated by the optimization process. The program is also able to optimize intermediate rendezvous and gravity assist or flyby trajectories of planets and small bodies. The class of Earth-Mars-Earth trajectory optimization problems is expected to have quite stable behavior; however the uniqueness of the problem, where the flyby would be performed in the lower layer of atmosphere below 80 km imposes some additional constraints which need to be addressed in the newly defined optimization problem. A special modification to the program was introduced to emulate the spacecraft velocity losses due to atmospheric drag associated with the low-altitude flyby portion of the trajectory. This provided an exceptional opportunity to optimize various AGA mission design scenarios based on the *Type I/II* and *Type III-IV*- incoming legs of the possible Mars sample return trajectories.

MIDAS, due to its patched-conic trajectory optimization capability, proved to be extremely effective as it quickly isolated trajectories that can be investigated further via high-fidelity integration programs. As an independent check, the optimization trajectory search strategy was also applied in MALTO¹⁶, a recently developed patched-conic trajectory optimization tool; however, unlike MIDAS, at that time the program did not have the capability to constrain the flyby *B-plane angle* of the incoming V_∞ vector which, in most cases, resulted in retrograde entries through the Martian atmosphere. These solutions have to be ignored from the list of potential EME aerogravity assisted trajectories due to substantial increase in atmospheric relative velocity at entry, $V_{am} > 7.5$ km/s which could be at the limit of a spacecraft thermal protection system design.

INTERPLANETARY TRAJECTORY DESIGN

The design metric as far as feasibility and optimality of the potential set of trajectories found in MIDAS was the overall mission ΔV . This was the natural choice, since any future mission which might utilize these results would depend heavily on the propulsive ΔV available per the spacecraft design. All of the EME candidate trajectories required a post-aeropass Deep Space Maneuver (DSM) to restore heliocentric energy and period of the spacecraft for the Earth return portion of the trajectory. Figure 3 illustrates some families of EME optimal trajectories found via the patched-conic approximation method. As seen in the graph, the required deterministic ΔV could be as low as 28.7 m/s and as high as 4 km/s.

The next stage in the trajectory design process was to select two or three promising trajectory solutions found by MIDAS and reoptimize them with software which supports the numerical integration of multi-body equations of motion to accurately model the spacecraft trajectory dynamics. This was accomplished using CATO¹⁷, a well-established JPL MDNAV program which became the primary tool for missions like Cassini and Juno. CATO is a high-fidelity propagator/optimizer which supports N-gravitating bodies (planets, moon, and asteroids), N-by-M gravity harmonic fields for a selected body, solar radiation pressure, and planetary atmospheric drag force. This interactive program is designed to minimize the total deterministic ΔV required for a multiple-flyby trajectory. For a more detailed analysis it was decided to select EME

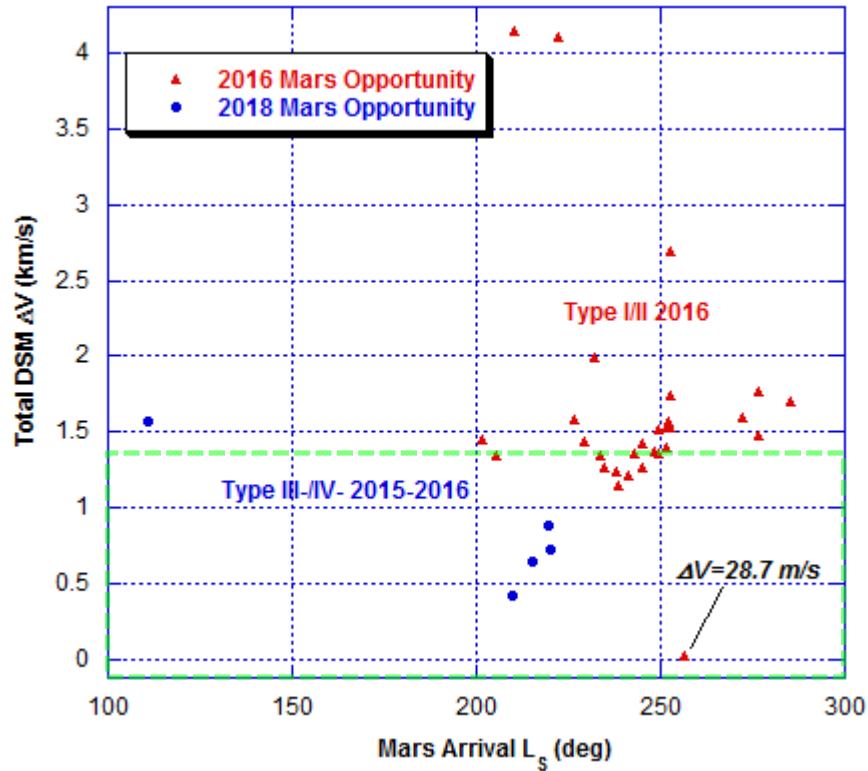


Figure 3. MIDAS Earth-Mars-Earth AGA optimal trajectories

trajectories with deterministic ΔV less than ~ 1 km/s (see Figure 3). However, to model the low-altitude flyby through the atmosphere it was essential to obtain a fairly characteristic density vs. altitude profile which would have a direct correlation to a particular Martian season. Special input parameter updates have been made to MarsGram 2005¹⁸ to produce the desired mean density profile which can be representative of 2016/2018 atmospheric conditions. More detailed discussion about the aeropass portion of a trajectory will be provided in the section called *Mars Aeropass Trajectory Analysis*. Table 1 illustrates various families of trajectories which have been methodically reoptimized in CATO based on the selected mean density profile. The table also provides a direct comparison with respect to the lifting AGA trajectory described in some previous publications¹⁰⁻¹¹.

The MIDAS patched-conic and CATO fully integrated trajectory results agreed fairly well. In most cases the optimum deterministic ΔV found via CATO trajectory design was slightly greater than MIDAS preliminary results by 30 to 40 m/s. The actual epoch of a DSM maneuver had to be moved in some cases by more than 60 days. The differences between the two approaches occur because that patched conic approach with ΔV_{drag} placed at Mars *periapsis* does not provide an accurate physical representation of atmospheric flyby, where a slight difference in Mars departure (post aeropass) V_{∞} vector, as was shown in CATO trajectories, can significantly change the optimum placement of the DSM ΔV maneuver.

Another challenge was to construct a 21-day launch period (LP) which would normally be required for any mission flown to Mars. For the trajectories listed in Table 1, the optimality of the MIDAS individual trajectories, which served as initial guesses for the CATO end-to-end integrated solutions, is highly dependent on the estimated drag losses which are inherently

Table 1. Possible 2016-2018 Mars sample return trajectories

Trajectory Type	Aeropass Type	Mars Arr. V_{∞}	Mars Aeropass	Venus Aeropass	Time of Flight	DSM ΔV (m/s)
Earth-Mars: Type I	<i>Ballistic</i>	5.85 km/s	2016 Aug 11	N/A	3 yrs 79 days	1455.1
Mars-Earth: Type IV-	<i>L/D =0</i>					
Earth-Mars: Type II	<i>Ballistic</i>	3.71 km/s	2016 Oct 10	N/A	3 yrs 112 days	1140.7
Mars-Earth: Type IV-	<i>L/D =0</i>					
Earth-Mars Type I	<i>Ballistic</i>	3.71 km/s	2016 Oct 14	N/A	3 yrs 26 days	1080
Mars-Earth: Type IV-	<i>L/D =0</i>					
Earth-Mars Type II	<i>Ballistic</i>	4.04 km/s	2016 Nov 7	N/A	4 yrs 74 days	76.5
Mars-Earth: Type V	<i>L/D =0</i>					
Earth-Mars Type I	<i>Ballistic</i>	4.75 km/s	2016 Nov 10	N/A	3 yrs 329 days	690.1
Mars-Earth: Type V	<i>L/D =0</i>					
Earth-Mars: Type III-	<i>Ballistic</i>	5.86 km/s	2018 Jan 6	N/A	4 yrs 56 days	1576.6
Mars-Earth: Type IV-	<i>L/D =0</i>					
Earth-Mars: Type IV-	<i>Ballistic</i>	5.04 km/s	2018 Jul 12	N/A	3 yrs 119 days	420
Mars-Earth: Type II	<i>L/D =0</i>					
Earth-Mars Type IV-	<i>Ballistic</i>	4.84 km/s	2020 Jun 10	N/A	3 yrs 307 days	1277.2
Mars-Earth: Type III-	<i>L/D =0</i>					
Earth-Mars Type I	<i>Lifting Trajectory</i>	7.95 km/s	2016 Jul 19	2017 Jan 25	1 yrs 134 days	None
Mars-Venus-Earth	<i>L/D =3</i>					

coupled with the Mars arrival V_{∞} magnitude. It was observed that within a constructed 21-day launch period, the arrival V_{∞} magnitude may vary by 100 m/s. A new iterative scheme was required to reoptimize each trajectory within a selected launch period based on the incoming V_{∞} vector and magnitude; this process was later named the “drag matching technique.” DSENDS¹⁹, JPL software which is used primarily for 3-DOF and 6-DOF flight vehicle dynamics simulation during EDL or any other proximity operations, was selected for this step in part because it incorporates a dynamic link to MarsGram, which expedited the iterative process between MIDAS and made the aeropass drag loss predictions extremely efficient. Once a more refined value of ΔV_{drag} was obtained from DSENDS simulations for each trajectory within a preliminary selected launch period, the MIDAS trajectory runs were repeated with more reliable ΔV_{drag} drag loss estimates associated with aeropass. The iterative analysis also assumed that the entry vehicle would have a ballistic coefficient of $\beta=2617.7 \text{ kg/m}^2$. The optimum solutions were further refined using the CATO high-fidelity trajectory integrator. Hence, in the global sense, based on the assumed mean density profile for Mars low-altitude atmospheric flyby, one can construct an optimum Earth-Mars-Earth trajectory where the resulting atmospheric drag losses would physically act as a “free,” propellant-less ΔV maneuver for optimum Spacecraft-Earth phasing for their orbit crossings. This would not eliminate the need for a Deep Space Maneuver (DSM) which could vary from 76.5 to 1277.2 m/s depending on opportunity, yet it should be emphasized that in a drag-free Mars flyby (i.e., assuming the flyby altitude is identical to aeropass scenario), the day-side flyby bends V_{∞} inward, lowering the orbital energy and period. The DSM in this case would add energy and increase the period for Earth-Spacecraft phasing. As drag increases, the outbound (departure) V_{∞} is smaller and the resultant spacecraft heliocentric velocity is larger relative to the $\Delta V_{drag}=0 \text{ m/s}$ case (see Figure 4). Hence, the DSM ΔV required to increase the spacecraft orbital period would be smaller. In the nominal Earth-Mars-Earth trajectory, the right amount of drag losses work in conjunction with the DSM to reduce the overall sample return mission ΔV . The off-nominal conditions will start to demonstrate some ΔV penalties. Hence, at lower flyby altitudes, the DSM ΔV starts to grow rapidly due to the fact that spacecraft heliocentric velocity

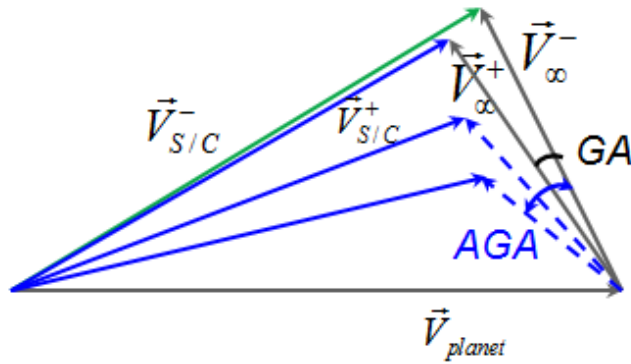


Figure 4. GA and AGA comparison for day-side planetary flyby

($V_{S/C}$) is getting large enough that the orbit would no longer cross Earth's orbit and, as the optimum trajectory techniques suggested, one DSM could no longer efficiently accomplish Spacecraft-Earth phasing, while two DSMs placed at *perihelion* and *aphelion* should generally lower the overall mission ΔV cost. This phenomenon is clearly illustrated in Figure 5 where for this example EME trajectory the optimum drag losses during the aeropass correspond to a Mars *periapsis* altitude of 42 km. The detailed analysis of a flyby altitude vs. DSM ΔV maneuver sensitivity and investigation of upper/lower bounds of an aeropass corridor driven by navigation and aerodynamic/atmospheric uncertainties will be described in the following sections.

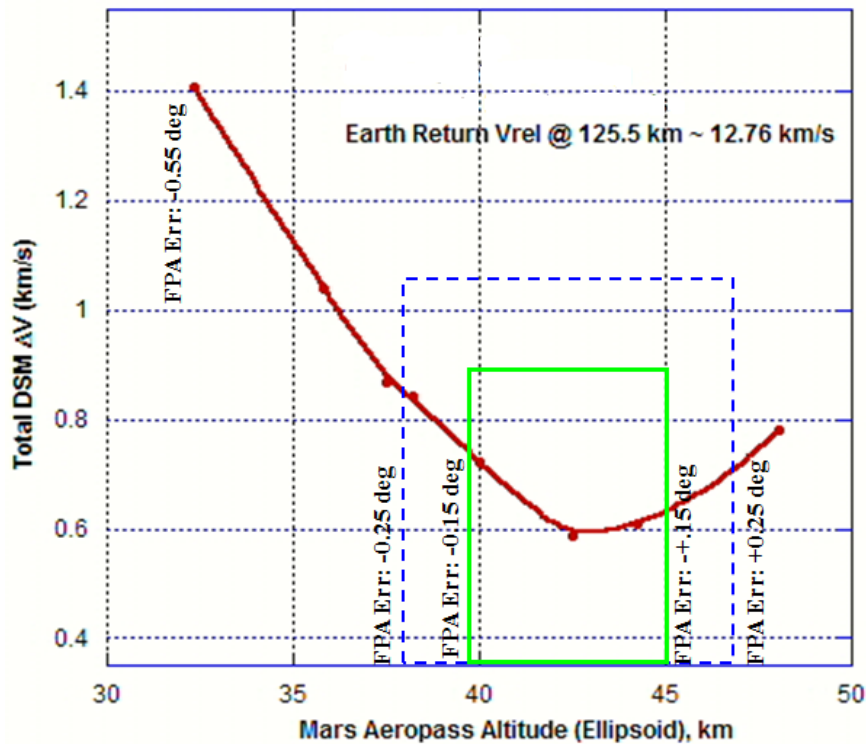


Figure 5. DSM ΔV Penalties versus flyby altitude

MARS AEROPASS TRAJECTORY ANALYSIS

The success of a future atmospheric sample return mission would highly dependent upon accurate spacecraft approach navigation and well-understood and robust flight vehicle dynamics during the aeropass maneuver. The entry flight path angle uncertainty is one of the most critical parameters for establishing an aeropass corridor and, ultimately, the bounds of expected drag losses which have a direct impact on the DSM ΔV magnitude and its location along the Earth return portion of a trajectory. The number of Orbit Determination (OD) measurements and data tracking types (e.g., DSN two-way Doppler, range, and ΔDOR) combined with the spacecraft configuration would dictate the EFPA knowledge and delivery errors at the Mars entry interface.

Since this is a conceptual study for which a spacecraft architecture was not defined, a comparison was made between a three-axis stabilized spacecraft with unbalanced thrusters (i.e., dead-banding for thruster control) and a similar spacecraft equipped with reaction wheels. A preliminary error assessment suggests that with five trajectory correction maneuvers on the Earth-Mars leg, where TCM-5 was placed at E-2 days or E-1 day, the flight path angle uncertainties exceeded $\pm 0.4^\circ$ (3σ) which retranslated into an aeropass corridor width greater than 8 km. A significant spread in drag losses resulted in DSM ΔV magnitude increase of 1.6 km/s, which might be at the limit of spacecraft propulsive capability.

The approach navigation analysis was repeated for some potential EME trajectories listed in Table 1 and a summary of these results is presented in Table 2 which shows that with the same TCM schedule and data tracking strategy (i.e., DSN two-way Doppler, range, and ΔDOR) applied to these four cases the EFPA 3σ uncertainty based on TCM-5 at E-2 days could be reduced to $\pm 0.11^\circ$.

Table 2. 2016-2018 Mars Approach Navigation Comparison

Trajectory Type Earth-Mars	2015 Type IV-	2017 Type IV-	2016 Type I	2016 Type I	
Mars Arrival Epoch	12-July-2018 23:58:57 ET	09-Jun-2020 23:59:58 ET	05-Nov-2016 23:55:23.34 ET	2016-10-12 23:57:27.88 ET	
Flight Path Angle $\pm 3\sigma$ reqt	-11.06° \pm 0.3°	-10.97° \pm 0.3°	-11.72° \pm 0.3°	-10.68° \pm 0.3°	
	TCM4@ENC – 8days				
Semi-major/minor Axis (3σ)	8.97/8.76 km	9.91/9.00 km	10.85/8.79 km	10.54/9.32 km	
Ellipse Orientation	39.9°	75.2°	111.7°	115.6°	
Linearized Flight Time (3σ)	1.70 sec	1.86 sec	1.95 sec	2.43 sec	
Entry Time (3σ)	6.77 sec	7.04 sec	6.69 sec	7.92 sec	
Entry Flight Path Angle (3σ)	0.54°	0.54°	0.52°	0.50°	
	TCM 5@ENC – 1day		TCM5@ENC – 2days		
Semi-major/minor Axis (3σ)	1.33/0.84 km	2.15/1.21	2.97/1.83	3.31/1.48 km	2.86/1.77 km
Ellipse Orientation	45.6°	73.7°	76.3°	114.3°	126.1°
Linearized Flight Time (3σ)	0.14 sec	0.15 sec	0.29 sec	0.45 sec	0.54 sec
Entry Time (3σ)	0.86 sec	0.95 sec	1.43 sec	1.45 sec	1.40 sec
Entry Flight Path Angle (3σ)	0.07°	0.08°	0.11°	0.11°	0.10°

A Type I Earth-Mars trajectory with an assumed launch date of April 3 and which would return the atmospheric sample to Earth on April 29, 2019 after completing an aeropass at Mars (see Figure 6) was selected for more detailed investigation. This trajectory does not have the smallest ΔV among other possible trajectory solutions listed in Table 1, but its short flight time makes it a top candidate for future mission selection. To understand the coupling effect between the navigation entry errors, Mars atmospheric, and vehicle aerodynamic uncertainties, a Monte

Carlo analysis was performed using POST²⁰, a program developed by NASA Langley Research Center (LaRC) for 3-DOF and 6-DOF trajectory simulations. As opposed to lifting AGA trajectories, the spacecraft would perform a simple ballistic entry with no active guidance during the aeropass maneuver. For the purpose of this study, it is assumed that the vehicle would be dynamically stable during the aeropass, where the forward C.G. location guarantees that the vehicle should not experience an angle of attack greater than 5°.

POST simulations rely heavily on the LaRC-developed Aerodynamics Database which provides drag and other aerodynamic coefficients as a function of Mach number and vehicle angle of attack (AOA). The aeropass Monte Carlo trajectory simulations assumed that the vehicle would have a ballistic coefficient of $\beta=2617.7 \text{ kg/m}^2$.

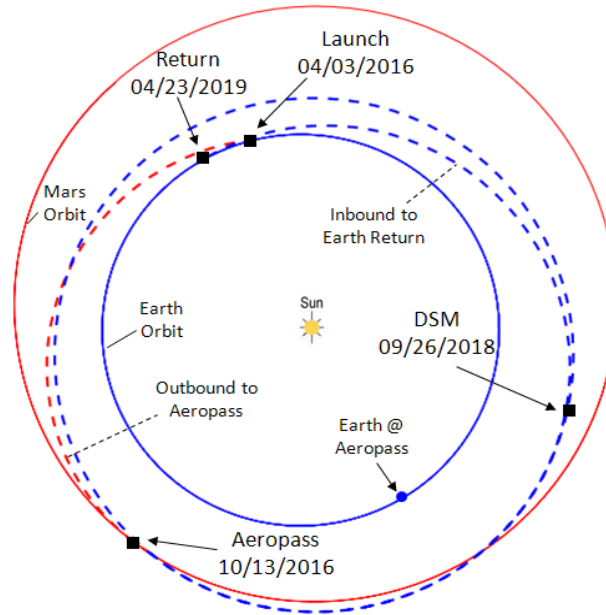


Figure 6. 2016 Earth-Mars-Earth Reference Trajectory

Another important set of parameters which can directly affect the results of the aeropass Monte Carlo simulations is the modeling of the Martian atmosphere. Like DSENDs, POST implements a dynamic link to the MarsGram 2005 atmospheric database. To guarantee that the trajectory Monte Carlo simulations capture various entry atmospheric conditions, the optical depth (τ) was uniformly dispersed from $0.1 \leq \tau \leq 3.0$. The presence of dust particles in the atmosphere can potentially raise its temperature, where the density may increase in the upper layers of atmosphere and substantially decrease in the lower layers; this alone may cause a huge variation in the estimated range of drag losses.

In addition to providing some verification of the AGA design robustness and identifying the altitude limits of an aeropass corridor, the POST Monte Carlo analysis provides an estimate of the extreme heat rates and loads which the vehicle might experience during the aeropass. These results can be used as a starting point for a future aerothermal analysis and are valuable when designing the Thermal Protection System (TPS). The peak heat rates and loads are computed based on the Sutton-Graves²¹ convective heat flux model

$$\dot{q} = k \sqrt{\frac{\rho}{r_n}} V_{atm}^3,$$

where $k = 1.9027 \times 10^{-4}$, which corresponds to a gas composition of 85% CO₂ and 15% N₂ and r_n is a vehicle nose radius. Based on the approach navigation analysis (Table 2), a detailed Monte Carlo analysis was completed for October 13, 2016 arrival conditions. Figures 7 through 10 provide a summary of 6-DOF simulation results for this aeropass opportunity. It is essential to point out that in the nominal case (Figure 7) the angle of attack does not exceed 0.5°, and even in dispersed trajectory scenarios the angle of attack would still be within the predicted limit of 5°. Other aeropass scenarios for various Mars arrival conditions in 2016-2020 opportunities have been analyzed based on the selected set of optimum trajectories outlined in Table 2. A complete summary of the 3-DOF Monte Carlo results is presented in Table 3.

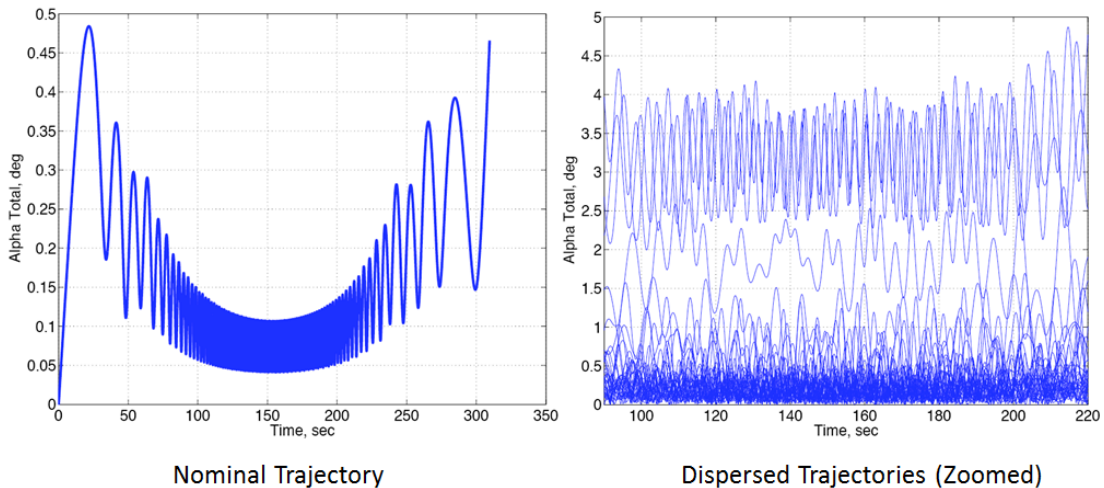
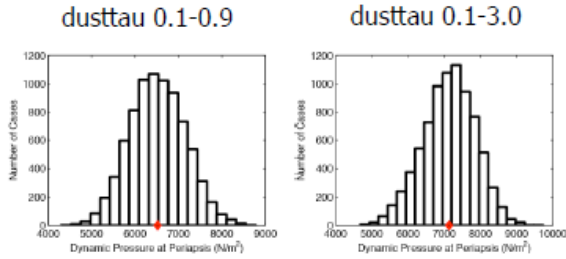


Figure 7. Angle of Attack α limits during the aeropass maneuver

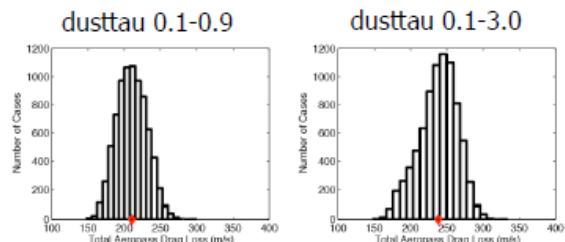
6 DOF Results



Statistics for
Dynamic Pressure at Periapsis (N/m²):

Mean = 6519.4115	Mean = 7134.1729
1-Sigma = 634.3496	1-Sigma = 720.8136
3-Sigma = 1903.0488	3-Sigma = 2162.4409
Minimum = 4303.1298	Minimum = 4678.906
00.13 %-tile = 4760.399	00.13 %-tile = 5055.3191
50.00 %-tile = 6507.9966	50.00 %-tile = 7166.5329
99.87 %-tile = 8392.6112	99.87 %-tile = 9062.1519
Maximum = 8776.9641	Maximum = 9733.6993
Min. Case = 7354	Min. Case = 482
Max. Case = 909	Max. Case = 7261

6 DOF Results

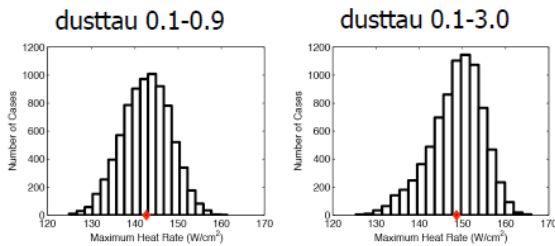


Statistics for
Total Aeropass Drag Loss (m/s):

Mean = 210.3871	Mean = 238.2623
1-Sigma = 20.4875	1-Sigma = 26.1169
3-Sigma = 61.4625	3-Sigma = 78.3507
Minimum = 147.6928	Minimum = 148.4025
00.13 %-tile = 156.8016	00.13 %-tile = 164.1063
50.00 %-tile = 209.8391	50.00 %-tile = 240.6485
99.87 %-tile = 269.8741	99.87 %-tile = 304.0684
Maximum = 297.7538	Maximum = 332.7526
Min. Case = 2980	Min. Case = 2980
Max. Case = 1487	Max. Case = 1487

Figure 8. 6-DOF Monte Carlo Analysis (Dynamic Pressure and Drag losses)

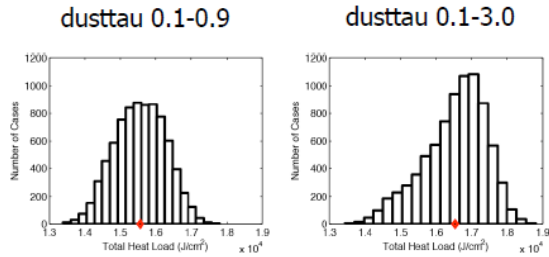
6 DOF Results



Statistics for
Maximum Heat Rate (W/cm²):

Mean = 142.634	Mean = 148.6504
1-Sigma = 5.5387	1-Sigma = 6.094
3-Sigma = 16.6161	3-Sigma = 18.2821
Minimum = 124.7357	Minimum = 125.3195
00.13 %-tile = 126.5526	00.13 %-tile = 128.5374
50.00 %-tile = 142.8089	50.00 %-tile = 149.3944
99.87 %-tile = 157.1888	99.87 %-tile = 162.7612
Maximum = 161.3263	Maximum = 165.936
Min. Case = 482	Min. Case = 68
Max. Case = 1487	Max. Case = 1487

6 DOF Results

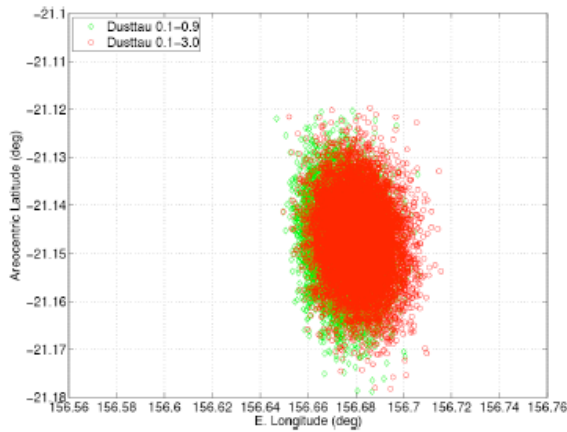


Statistics for
Total Heat Load (J/cm²):

Mean = 15557.5864	Mean = 16531.2285
1-Sigma = 711.6992	1-Sigma = 872.6985
3-Sigma = 2135.0977	3-Sigma = 2618.0956
Minimum = 13389.2118	Minimum = 13431.2383
00.13 %-tile = 13604.8166	00.13 %-tile = 13891.0671
50.00 %-tile = 15572.7776	50.00 %-tile = 16664.2823
99.87 %-tile = 17431.0244	99.87 %-tile = 18458.7127
Maximum = 17794.2794	Maximum = 18804.5369
Min. Case = 4101	Min. Case = 2980
Max. Case = 1487	Max. Case = 1487

Figure 9. 6-DOF Monte Carlo Analysis (Maximum Heat Rate/Load)

3 DOF Results



6 DOF Results

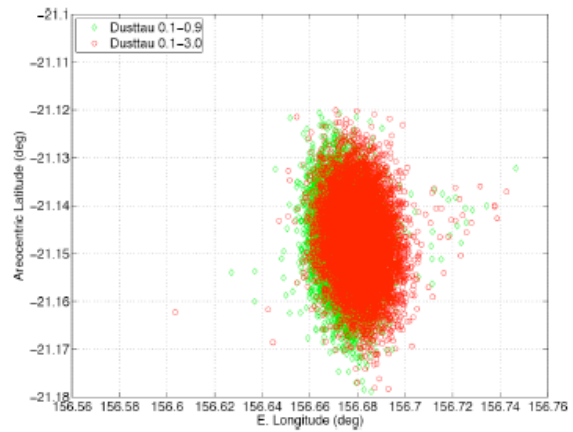


Figure 10. Exit conditions based on 3-DOF and 6-DOF Monte Carlo Results

Table 3. 3-DOF POST Monte Carlo Results

		2017 Type IV Trajectory		2016 Type I Trajectory		2016 Type I Trajectory (Encounter Updt)	
		dusttau 0.1 - 0.9	dusttau 0.1 - 3.0	dusttau 0.1 - 0.9	dusttau 0.1 - 3.0	dusttau 0.1 - 0.9	dusttau 0.1 - 3.0
Periapsis Latitude (deg)	mean	-8.02	-8.02	-49.27	-49.27	-21.15	-21.15
	+3 σ	-7.99	-7.99	-49.23	-49.23	-21.12	-21.12
	-3 σ	-8.05	-8.05	-49.30	-49.30	-21.17	-21.17
Entry Flight Path Angle (deg)	mean	-10.97	-10.97	-11.72	-11.72	-10.68	-10.68
	+3 σ	-10.85	-10.85	-11.61	-11.61	-10.58	-10.58
	-3 σ	-11.08	-11.08	-11.83	-11.83	-10.78	-10.78
Drag Loss (m/s)	mean	197.22	216.73	304.10	333.64	211.03	239.22
	+3 σ	256.51	279.75	381.90	424.85	271.52	315.81
	-3 σ	137.94	153.71	226.30	242.43	150.55	162.64
Max Heat Rate (W/cm ²)	mean	181.52	186.88	225.49	231.61	140.20	146.16
	+3 σ	203.44	207.89	247.60	254.54	156.34	163.72
	-3 σ	159.60	165.87	203.38	208.69	124.05	128.60
Total Heat Load (J/cm ²)	mean	17179	18071	22313.00	23453.77	15568.56	16550.98
	+3 σ	19658	20683	25036.11	26643.30	17668.46	19104.08
	-3 σ	14700	15459	19589.89	20264.25	13468.65	13997.88

SUMMARY AND CONCLUSIONS

A patched-conic MIDAS mission design program proved to be extremely efficient for a preliminary broad search of potential Mars atmospheric sample return trajectories. An iterative process between MIDAS, DSENDS and CATO simulations using a drag-loss matching strategy helped to quickly optimize the end-to-end integrated EME trajectories. In general, if the aeropass drag losses are within the assumed bounds, the optimum trajectories found in MIDAS and CATO agree well. The 3-DOF and 6-DOF Monte Carlo results of the vehicle aeropass have proven the robustness (i.e., 3 σ high AOA<5°) of the ballistic, unguided AGA design, where the navigation

EFPA 3σ uncertainty is the most critical parameter for establishing the upper and lower bounds of the aeropass corridor. It was also observed that higher values of τ result in increased drag losses, but have minimal effect on heating and G-loads.

ACKNOWLEDGMENTS

The research described in this paper was financially supported by the Jet Propulsion Laboratory, California Institute of Technology, under contract with the National Aeronautics and Space Administration. The Mars atmospheric entry analysis was performed at NASA Langley Research Center. A great degree of appreciation is given to JPL inner planetary navigation group for supporting this study. Special thanks to Carl Sauer and Larry Bright for making all the necessary enhancements to the legacy FORTRAN based mission design software MIDAS and CATO. An enormous degree of appreciation is given to David Skulsky and Liliya Dikin for making numerous editorial changes to this paper.

NOMENCLATURE AND ACRONYMS

AGA = Aero-Gravity Assist

AOA = Angle of attack

B-Plane = A plane normal to the incoming asymptote of the hyperbolic trajectory

CATO = Computer Algorithm for Trajectory Optimization

C_d = Drag coefficient

C.G = Center of gravity

DOF = Degrees of freedom

DSENGS = Dynamics Simulator for Entry, Descent and Surface landing

DSM = Deep Space Maneuver

DSN = Deep Space Network

E = Time from Entry Epoch (i.e. E-2 days)

EDL = Entry Descent and Landing

EFPA = Entry Flight Path Angle, deg

EME = Earth-Mars-Earth trajectory

GA = Gravity Assisted Trajectory

JPL = Jet Propulsion Laboratory

LaRC = Langley Research Center

L/D = Vehicle lift to drag ratio

LP = Launch Period

L_S = Solar longitude, deg

MALTO = Mission-Analysis Low-Thrust Optimization

MarsGram = Mars Global Reference Atmospheric Model
MC = Monte Carlo simulations
MIDAS = Mission Design and Analysis Software
MDNAV = Mission Design and Navigation
MSL = Mars Science Laboratory
MSR = Mars Sample Return
OD = Orbit Determination
periapsis = the distance of a closest approach to a planet
POST = Program to Optimize Simulated Trajectories
S/C = Spacecraft
TCM = Trajectory Correction Maneuver
TOF = Time of Flight
TRL = Technology Readiness Level
Type I = Heliocentric trajectory with transfer angle < 180 deg
Type II = Heliocentric trajectory with 180 deg < transfer angle < 360 deg
Type III- = Heliocentric trajectory (short period) with 360 deg < transfer angle < 540 deg
Type IV- = Heliocentric trajectory (short period) with 540 deg < transfer angle < 720 deg
 V_{atm} = Atmospheric relative velocity
 V_{∞} = Hyperbolic Excess Velocity
 V_{rel} = Planet-relative velocity magnitude
 $V_{S/C}$ = Spacecraft heliocentric velocity
 ΔDOR = Delta differential one way range
 ΔV = Change in Velocity during the Interplanetary transfer
 α = Angle of attack, deg
 β = Ballistic coefficient, kg/m²
 k = Sutton-Graves constant based on the gas composition
 τ = Optical depth parameter
 \dot{q} = Convective heat rate, W/cm²
 ρ = Atmospheric density
 r_n = Vehicle nose radius

REFERENCES

¹Bonfiglio, E. P., Longuski, J. M., and Vinh, N. X., "Automated Design of Aerogravity-Assist Trajectories," *Journal of Spacecraft and Rockets*, Vol. 37, No. 6, November-December 2000, pp. 768–775.

- ²Bonfiglio, E.P., “Automated Design of Gravity Assist and AeroGravity Assist Trajectories”, Purdue University Master’s Thesis in Aeronautics and Astronautics, Aug. 1999.
- ³Wyatt R. Johnson and James M. Longuski, “Design of Aerogravity-assist Trajectories”, AIAA-2000-4031, *AIAA/AAS Astrodynamics Specialist Conference*, Denver, CO, Aug. 14-17, 2000.
- ⁴Lewis, M. J., “The Use of Hypersonic Waveriders for Aero-Assisted Orbital Maneuvering,” *Proceeding of the 30th International Conference on Aviation and Space*, February 1990.
- ⁵Lewis, M.J., and McRonald, A.D., “The Design of Hypersonic Waveriders for Aero-Assisted Interplanetary Trajectories,” *Journal of Spacecraft and Rockets*, Vol.29, No.5, 1992, pp.653–660.
- ⁶McRonald, A. D., Randolph, J. E., “Hypersonic Maneuvering to Provide Planetary Gravity Assist,” AIAA Paper No. 90-0539, 1990.
- ⁷Gillum, M. J. and Lewis, M. J., “Analysis of Experimental Results on a Mach 14 Waverider with Blunt Leading Edges,” *Journal of Aircraft*, Vol. 34, No. 3, May 1997, pp. 296–303.
- ⁸Gillum, M., Kammeyer, M., Burnett, D., “Wind Tunnel Results for a Mach 14 Waverider,” *AIAA Paper* No. 94-0384, 1994.
- ⁹Casoliva, J., Lyons, D. T., Wolf A. A. and Mease, K. D., “Robust Guidance via a Predictor-Corrector Algorithm with Drag Tracking for Aero-Gravity Assist Maneuvers,” *AIAA Guidance, Navigation, and Control Conference and Exhibit*, Honolulu, Hawaii, August 18-21 2008, pp. 1-18.
- ¹⁰Lyons, D. T., Sklyanskiy, E., Casoliva, J., and Wolf, A. A., “Parametric Optimization and Guidance for an Aero-Gravity Assisted Atmospheric Sample Return From Mars and Venus,” *AIAA/AAS Astrodynamics Specialist Conference*, Honolulu, Hawaii, August 18-21 2008.
- ¹¹Lyons, D. T. and Sklyanskiy, E., “Interplanetary Waveriders for Atmospheric Sample Return,” *AAS Astrodynamics Specialist Conference*, Mackinac Island, Michigan, August 19-23 2007, pp. 1-20.
- ¹²Casoliva, J. and Mease, K. D., “Atmospheric Guidance for Aero-Gravity Assist Using Matched Asymptotic Expansions,” *AIAA/AAS Astrodynamics Specialist Conference and Exhibit*, Keystone, Colorado, August 2006.
- ¹³Schlaifer, S., Rinderle, E., Skinner, D., “XCOUNT User’s Guide”, 2006.
- ¹⁴Planetary Mission Entry Vehicles Quick Reference Guide, Version 3.0 NASA/SP-2006-3401
- ¹⁵Sauer, C. G., Jr., “MIDAS – Mission Design and Analysis Software for the Optimization for Ballistic Interplanetary Trajectories,” *Journal of the Astronautical Sciences*, 37, 1989, pp. 251-259.
- ¹⁶Kowalkowski, T.D., Rinderle, E. A., Landau, D. F., “Mission-Analysis Low-Thrust Optimization (MALTO) User’s Manual,” Version 5.2.6, July 2008.
- ¹⁷Byrnes, D.V., and Bright, L.E., “Design of High-Accuracy Multiple Flyby Trajectories Using Constrained Optimization,” *AAS/AIAA Astrodynamics Specialist Conference*, Halifax, Nova Scotia, Canada, August 1995.
- ¹⁸Justh, H., Keller, V., “Mars Global Reference Atmospheric Model 2005 (Mars-GRAM 2005) User’s Guide,” December 2005.
- ¹⁹Balaram, B., “Dynamics Simulator for Entry, Descent and Surface landing (DSEDS) User’s Guide,” September 2010.
- ²⁰Brauer, G. L., Cornick, D. E., and Stevenson, R., “Capabilities and Applications of the Program to Optimize Simulated Trajectories (POST),” NASA CR-2770, Feb. 1977.
- ²¹Sutton, K. and Graves Jr., R. A., “A General Stagnation Point Convective Heating Equation for Arbitrary Gas Mixtures,” Tech. Rep. TR-R376, NASA, November 1971.